High Precision Model Predictive Power Control Method for Battery Energy-Stored Quasi Z-Source Inverter

Yi Liu, *Member, IEEE*, and Jia Jia Li, *Member, IEEE*

***Abstract*—The battery energy-stored quasi Z-source inverter (BES-qZSI) is widely used for photovoltaic power generation system to suppress the fluctuation in photovoltaic power. With the model predictive control, the photovoltaic power generation system obtains a good performance in dynamic response. However, the control accuracy is affected by the sampling frequency because of one voltage vector applied very control cycle. In this article, a high precision model predictive power control method is proposed for the BES-qZSI to reduce the power fluctuation from the perspective of reforming the quality of dc-side inductor current and output current. The deadbeat control is modified to control the inductor current, so that the inductor current can track its reference command precisely with lower ripple. The dual-vector model predictive control is applied by expanding the voltage vector combination. The voltage vector inverter with higher phase freedom degree is applied to inverter, improving the control accuracy of the output current. The experimental results verify the validity and the advantages of the proposed method.**

***Index Terms*—Battery energy-stored quasi z-source inverter (BES-qZSI), control accuracy, model predictive control, photovoltaic power generation system.**

I. Introduction

THE output power of photovoltaic cells undergoes a real-time change with the solar radiation intensity and environmental temperature, worsening the grid connection characteristics of the inverter [1], [2]. To suppress fluctuations in photovoltaic power generation, energy storage battery units can be used into photovoltaic power generation systems. The energy storage battery unit is usually connected to the photovoltaic power generation system through a bidirectional dc–dc converter [3], [4], [5]. The photovoltaic power generation system based on battery energy-stored quasi Z-source inverter (BES-qZSI) directly parallels the energy storage battery units at both ends of two capacitors qZSI [6]. The BES-qZSI has the abilities to balance the photovoltaic power and the required power of the grid and suppresses the impact of random fluctuations in photovoltaic power on the grid. Moreover, the unique shoot-through state enables the BES-qZSI to achieve both dc–dc and dc–ac in a single stage system. With the advantages of high integration, efficiency, gain, and reliability, the BES-qZSI has great prospects in the field of photovoltaic power generation [7], [8].

In photovoltaic power generation system, the BES-qZSI systems is usually controlled by a proportional integral differential (PID) regulator, and thus a shoot-through state can be inserted into space vector modulation algorithm to achieve output power regulation [9], [10]. In addition, some nonlinear control methods are also applied to BES-qZSI systems, such as sliding mode control and PR control. In spite of achieving multi-objective control of BES-qZSI in photovoltaic power generation system, the linear PID control has the drawbacks of complex controller parameter design, slow dynamic response, and the need of pulsewidth modulation (PWM) modulator. With the rapid development of powerful microprocessors, finite control set model predictive control (FCS-MPC) has gained much attention in the fields of power electronics [11], [12], [13], [14], [15]. FCS-MPC has the characters of no PWM modulator, simple structure, easy implementation, and fewer tuning parameters. Hence, fast dynamic response and handling of multiple variables in photovoltaic power generation system can be easily achieved by FCS-MPC.

A FCS-MPC strategy for the BES-qZSI was proposed in [16]. The precise control and fast tracking of multiple variables can be realized simultaneously. In [17], the algorithm of FCS-MPC was improved by adjusting the conditions for shoot-through state selection, simplifying the cost function and reducing computational complexity. In [18], a switching frequency constraint strategy is used to the FCS-MPC for the BES-qZSI. The influence of weighting factor on switching frequency and total harmonic distortion (THD) is analyzed in detail. However, as only one switch state is applied during each control cycle, the control effect of FCS-MPC heavily depends on sampling frequency. In addition, inconstant switching frequency and the irregular distribution of current harmonics are not conducive to filter design.

To reduce the influence of unfixed switching frequency and sampling frequency on maximum power point tracking accuracy, the model predictive current control with finite switching

Manuscript received 23 November 2023; revised 18 March 2024; accepted 10 May 2024. Date of publication 16 May 2024; date of current version 20 June 2024. This work was supported in part by the Industry University Research Cooperation Project of Jiangsu Province under Grant BY20230961. Recommended for publication by Associate Editor S. S. Williamson. *(Corresponding author: Yi Liu.)*

Yi Liu is with the Institute of Building Intelligence, Jiangsu Vocational Institute of Architectural Technology, Xuzhou 221008, China (e-mail: 11027@jsviat.edu.cn).

Jia Jia Li is with the College of Electrical and Control Engineering, Henan University of Urban Construction, Pingdingshan 467036, China (e-mail: 20151015@huuc.edu.cn).

Color versions of one or more figures in this article are available at https://doi.org/10.1109/TPEL.2024.3402056.

Digital Object Identifier 10.1109/TPEL.2024.3402056

sequence for the BES-qZSI becomes more and more attractive. In [19], the idea of logical control is adopted to control the charging and discharging time of the inductor current, avoiding large inductor current ripple. In [20], a joint voltage vector based FCS-MPC was proposed to suppress the inductor current and output current ripples of the converter, reducing the THD of the output current. However, the current reference command calculated by the deadbeat control method causes a control error in the output power. In [21], a finite switching sequence model predictive current control strategy was proposed. The grid current is precisely controlled under a fixed switching frequency with lower sampling frequency, good dynamic and steady-state performance. In [22], combined FCS-MPC with direct power control algorithms, a finite switching sequence model predictive direct power control strategy was proposed. Both neutral-point balancing control and optimal control of active and reactive power on the ac side are achieved.

This article proposes a high-precision model predictive power control method for the BES-qZSI to address the impact of the power fluctuation of photovoltaic cells on the power grid. The principles of deadbeat control and extended dual-vector model predictive control are used to improve the control accuracy of output power from the perspective of reforming the quality of dc-side inductor current and output current of the BES-qZSI. First, a predictive model of the BES-qZSI is derived by its mathematical model. Second, the operation time of shoot-through voltage vector and non- shoot-through voltage vector is calculated based on deadbeat control to ensure the average inductor current is equal to the reference command of inductor. In consequence, the voltage of the capacitor paralleled with the battery is stable, which is the precondition of output power control. Finally, by expanding the candidate voltage vector combinations associated with the target voltage vector, the control accuracy of the output control current as well as the output power is improved. The experimental results verify the correctness and effectiveness of the proposed method.

The rest of this article is organized as follows. In Section II, the prediction model of the BES-qZSI is deduced, and the FCS-MPC for the BES-qZSI is explicated. Section III is devoted to the description of the proposed method in detail, including the overall control structure, modified deadbeat control for inductor current, and extended dual-vector model predictive control for output current. In Section IV, the experimental results and analysis are presented. Finally, Section V concludes this article.

The contributions of this article are summarized as follows.

1) A modified deadbeat control is proposed to reduce the inductor current ripple and improve the control accuracy of inductor current.
2) An extended dual-vector model predictive control is proposed to increase the degrees of the amplitude and phase freedom of the output voltage, obtaining lower THD and higher quality of the output current.
3) The reason of the fluctuation in photovoltaic power caused by the BES-qZSI is revealed. Through reforming the quality of dc-side inductor current and output current, the efficiency of photovoltaic power generation is improved.

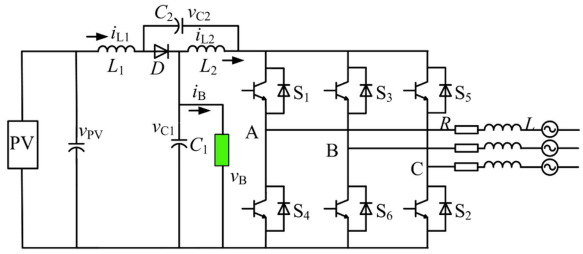

Fig. 1. Energy storage quasi Z-source photovoltaic grid connected inverter topology.

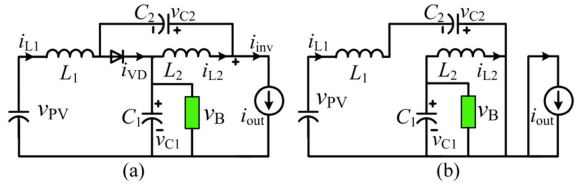

Fig. 2. Equivalent circuits of BES-qZSI in (a) non-ST state and (b) ST state.

II. Prediction Model of BES-qZSI

The structural diagram of the BES-qZSI is shown in Fig. 1, consisting of a photovoltaic cell unit, quasi Z-source inverter, RL load, energy storage battery, and power grid. The energy storage battery is equivalent to an ideal voltage source and internal resistance connected in series structure.

A. Prediction Model of BES-qZSI

The BES-qZSI has two working states, namely the non-shoot-through state and the shoot-through state. The equivalent circuits of the two working states of the BES-qZSI are shown in Fig. 2. In the shoot-through state of the BES-qZSI, the bridge arms are short circuited, and the current of the diode D is discontinuous. Therefore, there are three loops on the dc and ac-sides of the inverter, that is, the load freewheeling loop, the loop consisting of the inductor L_1, capacitor C_2, and power supply $v_{\rm PV}$, as well as the loop consisting of the inductor L_2 and capacitor C_1. On the dc-side, the inductors L_1 and L_2 are charged by the capacitors C_1 and C_2, respectively. In the nonshoot-through state, the capacitors C_1 and C_2, are charged by the power supply $v_{\rm PV}$ and inductors L_1 and L_2. The BES-qZSI works between the shoot-through and nonthrough-states, leading to dynamic balance of the discharging and charging currents of the inductor.

If the same inductances are selected for the inductors L_1 and L_2, the currents of the inductors L_1 and L_2 will be the same due to the principle of the BES-qZSI. The equivalent inductance brings benefit in the BES-qZSI design. Therefore, it is only necessary to derive prediction model of the current of inductor L_1 in the following circuit analysis.

The inductor current in the shoot-through state and the non-shoot-through state can be expressed as

$$L_1 \frac{di_{\rm L1}}{dt} = v_{\rm PV} + v_{\rm C2} \tag{1}$$

$$L_1 \frac{di_{\mathrm{L1}}}{dt} = v_{\mathrm{pv}} - v_{\mathrm{C1}} \tag{2}$$

where C_1 and L_1 are the capacitance and the inductance of the BES-qZSI, respectively. v_{pv}, v_{C1}, and v_{C2} are the input voltage of the BES-qZSI and the voltages of the capacitor C_1 and C_2, respectively. By using Euler method to discrete (1) and (2), the predicted inductor current is derived as

$$i_{\mathrm{L1}}(k+T_{\mathrm{s}}) = \frac{T_{\mathrm{s}}[v_{\mathrm{pv}} + v_{\mathrm{C2}}(k)]}{L_1} + i_{\mathrm{L1}}(k) \tag{3}$$

$$i_{\mathrm{L1}}(k+T_{\mathrm{s}}) = \frac{T_{\mathrm{s}}[v_{\mathrm{pv}} - v_{\mathrm{C1}}(k)]}{L_1} + i_{\mathrm{L1}}(k) \tag{4}$$

where k, T_{s}, and k-T_{s} are the current moment, the control period, and the last moment, respectively. The output voltage $v_{(\alpha,\beta)}$ can be expressed as

$$v_{(\alpha,\beta)} = \frac{2v_{\mathrm{pv}}(\mathrm{S}_1 + a\mathrm{S}_3 + a^2\mathrm{S}_5)}{3} \tag{5}$$

where a $= 1/2+\mathrm{j}\sqrt{3}/2$. S_1, S_3, and S_5 are the switching states of the inverter in different phases. The output voltage balance equation is given by

$$v_{(\alpha,\beta)} = L\frac{di_{(\alpha,\beta)}}{dt} + Ri_{(\alpha,\beta)} \tag{6}$$

where i_α and i_β are the components of the three-phase output currents in $\alpha\beta$ coordinate system; R and L are the resistance and the inductance of RL load. According to Euler method, the future value of the output current is expressed as follows

$$i_{(\alpha,\beta)}(k+T_{\mathrm{s}}) = \frac{T_{\mathrm{s}}v_{(\alpha,\beta)}(k+T_{\mathrm{s}}) + Li_{(\alpha,\beta)}(k)}{RT_{\mathrm{s}} + L}. \tag{7}$$

B. FCS-MPC for BES-qZSI

From the working principle of the BES-qZSI in Fig. 2, the BES-qZSI is able to boost the dc-side voltage and output desired sine current. Therefore, the inductor current, the capacitor voltage, and the output current should be selected as the control variables in the cost function.

The control variable errors between the predicted values and the references under basic VVs are evaluated by the following cost function to choose the optimal VV

$$\begin{aligned} g = {} & [i_{\alpha,\mathrm{ref}} - i_\alpha(k+T_{\mathrm{s}})]^2 + [i_{\beta,\mathrm{ref}} - i_\beta(k+T_{\mathrm{s}})]^2 \\ & + \lambda_C[v_{\mathrm{C1,ref}} - v_{\mathrm{C1}}(k+T_{\mathrm{s}})]^2 + \lambda_L[i_{\mathrm{L1,ref}} - i_{\mathrm{L1}}(k+T_{\mathrm{s}})]^2 \end{aligned} \tag{8}$$

where λ_C and λ_L are the weighting factors of the capacitor voltage and the inductor current, respectively. $i_{\alpha,\mathrm{ref}}$, $i_{\beta,\mathrm{ref}}$, $v_{C1,\mathrm{ref}}$, and $i_{L1,\mathrm{ref}}$ are the references of the three phase output currents on α and β coordinate axes, the capacitor voltage, and the inductor current, respectively. In (8), the inductor current, the capacitor voltage, and the output current have different importance to the qZSI control system, and thus weighting factors with different values are matched for the three controlled variables to distinguish their importance.

The weighting factors are mostly designed by the trial and error method. Thus, the weighting factors are adjusted according to the experimental results to ensure the performance balance of each variable. In the first step, the weighting factors are initially chosen. In the second step, the weighting factor of the inductor current is regulated to obtain a steady current ripple due to the experimental results. In the third step, the weighting factor of the capacitor voltage is regulated to obtain a desired dc-link voltage. In the fourth step, the weighting factor of the output current is tuned for obtaining a sine output current. The tuning process above is based on the experiences of a researcher.

III. High Precise Model Predictive Power Control Method

A. Control Structure of Proposed Method

External environmental factors such as light and temperature affect the maximum power point of the photovoltaic system. For the BES-qZSI, the inductor current and output current control is the key to achieving maximum power point tracking. How to improve the current control accuracy of the BES-qZSI is a current research challenge. Although FCS-MPC can improve the control accuracy of the current by predicting future states, one voltage vector applied within a long control cycle results in significant current ripple, which reduces tracking accuracy of maximum power point.

To address the problem of the power fluctuation of photovoltaic cells, this article proposes a high precision model predictive power control method. By analyzing the influence of each voltage vector on the controlled variables of the BES-qZSI, the optimal voltage vector combination for the inductor current and output current control can be obtained. The operation time of each selected voltage vector is calculated based on the principle of deadbeat control, achieving the significant error reduction of the inductor current and the output current.

The control structure of the proposed method mainly composed of three parts: BES-qZSI state prediction, modified deadbeat control for inductor current, and extended dual-vector model predictive control for output current, as shown in Fig. 3. The implementation is given as follows.

1) Sample the current state of the BES-qZSI, and then calculate the inductor current and the output current at the next moment by predictive model. The maximum input power of a photovoltaic panel varies with temperature and light intensity. The perturbation and observation method can detect the maximum output power of the photovoltaic panel and its corresponding output voltage. The linear regulator is employed to calculate the reference of the inductor current.
2) Take the shoot-through voltage vector and non- shoot-through voltage vector as candidate voltage vectors to control the inductor current. Use modified deadbeat control to calculate the action time of each vector and convert the action time into duty cycle.
3) Control the output current using the combination between the active voltage vector and zero voltage vector as well as the combination of multiactive vectors. Use the extended dual-vector model predictive control to calculate the optimal duty cycles of the two voltage vector combinations. By comparing the cost function of the synthesized voltage vector with that of the reference voltage vector, the optimal voltage vector combination can be selected.

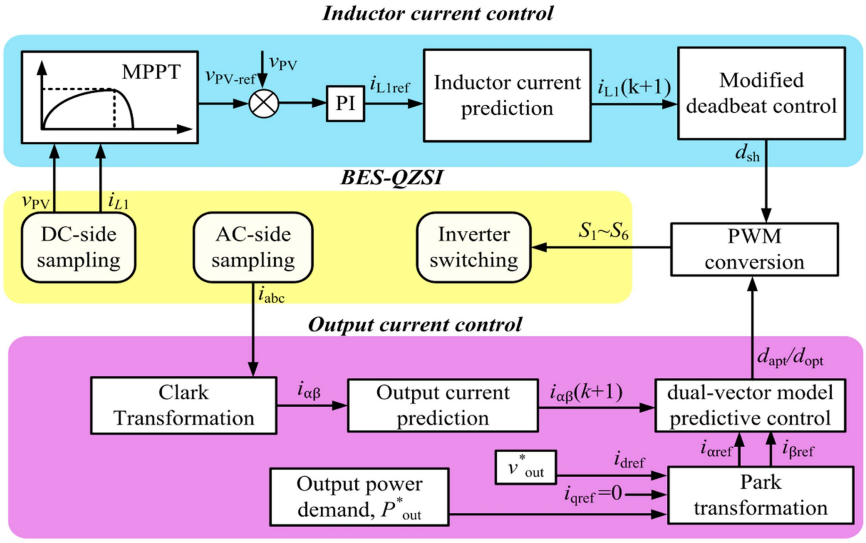

Fig. 3. Structure diagram of proposed method.

4) Convert the optimal voltage vector combination for controlling the inductor current and the output current into a PWM signal driving the EBS-qZSI.

B. Modified Deadbeat Control for Inductor Current

For the photovoltaic power generation system, the input power can be obtained by detecting the voltage of the photovoltaic ceils and the inductor current of the BES-qZSI. When the maximum power point of the photovoltaic module changed, the regulation of the inductor current, the output voltage, or both of the BES-qZSI should be exerted. Therefore, the inductor current plays an importance role for the maximum power point tracking.

The error of the controlled variable can be quickly eliminated within a limited control cycle by deadbeat control. The deadbeat control is often used in voltage source inverter and motor control. For the BES-qZSI, the power is related to the average value of inductor current rather than the instantaneous value of inductor current. Therefore, using deadbeat control to control the instantaneous value of inductor current will result in a mismatch between output power and maximum power, lowering the efficiency of photovoltaic power generation. In this section, a modified deadbeat control is proposed to achieve precise control of the average inductor current. The principle of the modified deadbeat control is employing a shoot-through voltage vector and a nonshoot-through voltage vector to ensure the average charging inductor current and the discharging inductor current equal the reference command of the inducer Current.

As the inductor current increases under the shoot-through voltage vector and decreases under the non-shoot-through voltage vector, it is convenient to control the ripple and error of the inductor current through applying a combination of the two voltage vectors. Under the condition of minimum inductor current ripple, a relationship between the predicted value and the reference command of the inductor current can be established based on the principle of deadbeat control. The solution of this relationship is the operation time of the shoot-through voltage vector and the non-shoot-through voltage vector. The solution process is given as follows.

Firstly, the change rates of the current of the inductor L_1 in the shoot-through state and non-shoot-through state are given by

$$S_{\rm sh} = \frac{i_{L1-{\rm sh}}(k+T_s) - i_{L1-{\rm sh}}(k)}{T_s} \tag{9}$$

$$S_{\rm nsh} = \frac{i_{L1-{\rm nsh}}(k+T_s) - i_{L1-{\rm nsh}}(k)}{T_s} \tag{10}$$

where $S_{\rm sh}$ and $i_{L1\text{-sh}}(k+T_s)$ are the change rate and the predicted value of the inductor current in the shoot-through state, respectively. $S_{\rm nsh}$ and $i_{L1\text{-nsh}}(k+T_s)$ are the change rate and the predicted value of the inductor current in the non-shoot-through state, respectively.

Second, the predicted inductor current using (9) and (10) are calculated as

$$i_{L1}(k+T_s) = i_{L1}(k) + S_{\rm sh}T_s d_{\rm sh} + S_{\rm nsh}T_s(1-d_{\rm sh}) \tag{11}$$

where $d_{\rm sh}$ is the duty ratio of the shoot-through state. To ensure obtaining the minimum error of the inductor current, the inductor current should be symmetrical about its reference command within a control cycle. The control law can be expressed as

$$i_{L1,{\rm ref}} - i_{L1}(k+T_s) = i_{L1}(k) + S_{\rm sh}T_s d_{\rm sh} - i_{L1,{\rm ref}} \tag{12}$$

where $i_{L1,{\rm ref}}$ is the reference command of the inductor current. By solving (12), the duty ratio of the shoot-through state are given by

$$d_{\rm sh} = \frac{2i_{L1,{\rm ref}} - 2i_{L1}(k) - S_{\rm nsh}T_s}{T_s(2S_{\rm sh} - S_{\rm nsh})}. \tag{13}$$

Fig. 4 shows the modified deadbeat control effect on the inductor current. In Fig. 4(a), it is assumed that the inductor current at start time is equal to the reference command. If the shoot-through voltage vector or the non-shoot-through voltage vector is applied throughout the entire control cycle, the average inductor current

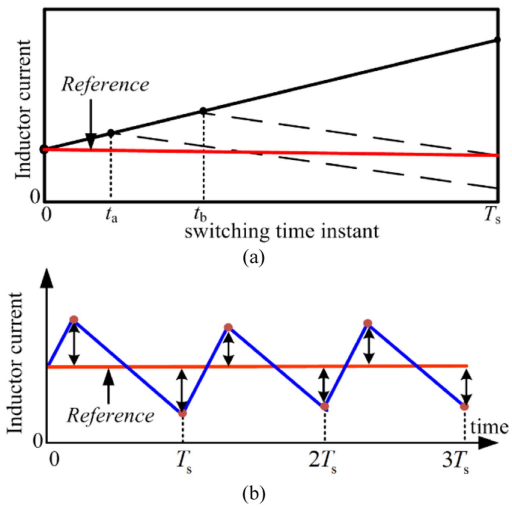

Fig. 4. Modified deadbeat control of inductor current. (a) Switching time instant. (b) Inductor current ripple.

is higher or lower than the reference command. Accordingly, the average inductor current can be regulated the use of the two voltage vector combination. According to the principle of deadbeat control, switching the shoot-through voltage vector and the non-shoot-through voltage vector at time instant t_b can ensure that the predicted value of the inductor current is equal to the reference command. However, the average inductor current is higher than the reference command, causing a large control error. If the switching time instant is t_a, the inductor current error is symmetrical with respect to the reference command of the inductor current. It can be seen that the inductor current error is reduced to half of that when the voltage vector is switched at time instant t_b.

When the initial inductor current coincides with the reference command, the effect of the modified deadbeat control is shown in Fig. 4(b). After a control cycle, it can be seen that: the inductor current is the same at the beginning and end of the control cycle; the positive and negative errors are symmetrical; and the ripples of the charging current and the discharging current are equal, meeting the principle of volt-second balance. Therefore, the inductor current error can be significantly reduced by the modified deadbeat control.

C. Extended Dual-Vector Model Predictive Control for Output Current

The EBS-qZSI has two approaches to track the maximum power point of the photovoltaic module, namely regulating the inductor current and the output current. In the following section, the modified deadbeat control for the inductor current is explicated. In Section IIII-C, an extended dual-vector model predictive control is given to improve the quality of the output current. Through the position location of the target voltage vector and the dual vector combination sequence expansion, the proposed method can improve the control accuracy of output current with low computational complexity.

When an active voltage vector is applied during a whole control error, the amplitude and the direction of the voltage vector are fixed. This article adopts an extended dual vector combination, including not only the combination of an active voltage vectors and a zero voltage vector, but also the combination of two active vectors. By comparing the different voltage vector combinations, one closed to the voltage vector reference will be selected as the output voltage vector. As a result, the combination of an active voltage vector and a zero voltage vector will be applied under the condition of the reference vector located in both sides of sector. While the combination of two active voltage vectors will be applied under the condition of the reference vector located in the center of sector. The implementation of the proposed method is given as follows.

The first step is to perform an equivalent current control that is converting the output current reference into output voltage reference. The application of the voltage vector close to the output voltage reference will generate the expected output current. The equivalent control facilitates the selection of proper voltage vector combination. According to (4), the predicted output voltage can be calculated

$$v_{(\alpha,\beta)}(k+T_s) = L\frac{i_{(\alpha,\beta)}(k+T_s)-i_{(\alpha,\beta)}(k)}{T_s} + Ri_{(\alpha,\beta)}(k+T_s). \quad (14)$$

According to deadbeat control principle, the output current and the output voltage at $k+T_s$ moment are equal to their references $v_{(\alpha,\beta),\mathrm{ref}}$ and $i_{(\alpha,\beta),\mathrm{ref}}$. By substituting $v_{(\alpha,\beta),\mathrm{ref}}$ and $i_{(\alpha,\beta),\mathrm{ref}}$ into (19), the output voltage reference is obtained as

$$v_{(\alpha,\beta),\mathrm{ref}} = L\frac{i_{(\alpha,\beta),\mathrm{ref}}-i_{(\alpha,\beta)}(k)}{T_s} + Ri_{(\alpha,\beta),\mathrm{ref}}. \quad (15)$$

From (15), it can be seen that a voltage vector with the same amplitude and direction as the reference voltage vector can ensure that the output current is consistent with its reference.

The second step is to calculate the duty ratio of the combination of active voltage vector and zero voltage vector as well as that of the combination of two active voltage vectors. The operation time of each vector will result in differences in the amplitude and phase of the synthesized vector. Therefore, it is necessary to calculate an optimal duty ratio to ensure that the synthesized vector is closest to the reference of the output voltage vector. The duty ratio of the combined vector can be obtained through the following cost function

$$g^2 = \left|v_{(\alpha,\beta),\mathrm{ref}} - d_{\mathrm{pt}}T_s v_{\mathrm{pt1}} - (1-d_{\mathrm{sh}}-d_{\mathrm{pt}})T_s v_{\mathrm{pt2}}\right|^2 \quad (16)$$

where v_{pt1} and v_{pt2} are the first and second voltage vectors of combined voltage vector, respectively. $d_{\mathrm{pt}}T_s$ is the action time of v_{pt1}, while $(1\text{-}d_{\mathrm{sh}}\text{-}d_{\mathrm{pt}})T_s$ is the action time of v_{pt2}. Equation (16) represents the error between the output voltage reference and the voltage vector synthesized by v_{pt1} and v_{pt2}.

According to the principle of extended dual-vector model predictive control, the optimization problem is using two different vectors to approach the reference voltage vector. Regardless of the form of vector combination, the amplitude and direction of the zero voltage vector and the six active voltage vectors are

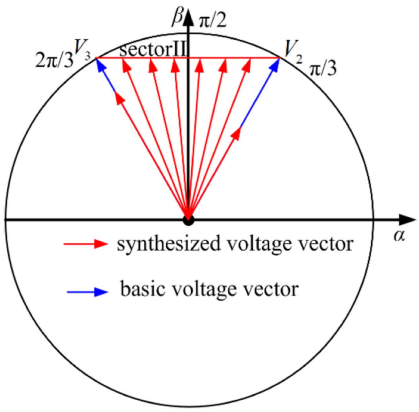

Fig. 5. Principle of extended dual-vector model predictive control.

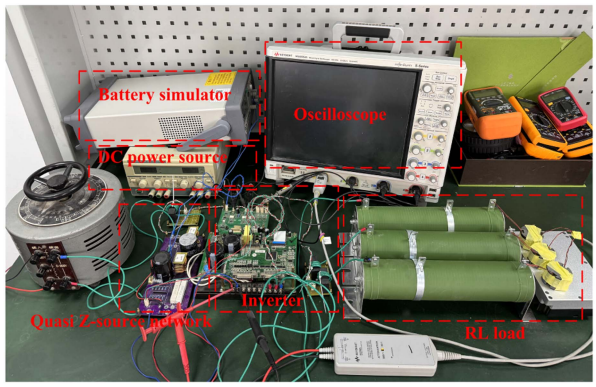

Fig. 6. Experiment platform of BES-qZSI.

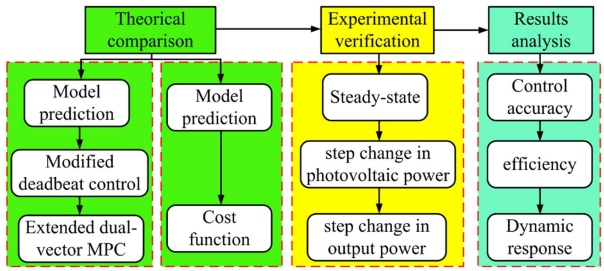

Fig. 7. Scheme of experimental research.

uniquely determined. Meanwhile, $d_{\rm sh}$ can be calculated from (13), and the control period $T_{\rm s}$ is also known. Therefore, only the duty ratio $d_{\rm pt}$ is a variable in (16) when the two voltage vectors are established. Equation (16) can be seen as a function of $d_{\rm pt}$. By calculating the derivative of the function g^2, the optimal duty ratio $d_{\rm pt}$ that minimizes g^2 can be obtained. The extreme value of the cost function g^2 can be obtained by setting

$$\frac{\partial\left(g^2\right)}{\partial d_{\rm pt}}=0. \tag{17}$$

By substituting (16) into (17), (17) is deduced as

$$\left|v_{(\alpha,\beta),\rm ref}-\right.$$
$$\left.d_{\rm pt}T_s v_{\rm pt1}-(1-d_{\rm sh}-d_{\rm pt})T_s v_{\rm pt2}\right|\left(-T_s v_{\rm pt1}+T_s v_{\rm pt2}\right)=0. \tag{18}$$

Equation (18) can be further derived as

$$d_{\rm pt}\frac{\left(T_s v_{\rm pt2}-T_s v_{\rm pt1}\right)^2}{\left(T_s v_{\rm pt1}-T_s v_{\rm pt2}\right)}=\left[v_{(\alpha,\beta),\rm ref}-(1-d_{\rm sh})T_s v_{\rm pt2}\right]. \tag{19}$$

According to (19), the optimal duty ratio $d_{\rm pt}$ can be expressed as

$$d_{\rm pt}=\frac{\left[v_{(\alpha,\beta),\rm ref}-(1-d_{\rm sh})T_s v_{\rm pt2}\right]\left(v_{\rm pt1}-v_{\rm pt2}\right)}{T_s\left(v_{\rm pt2}-v_{\rm pt1}\right)^2}. \tag{20}$$

The third step is to choose the optimal voltage vector combination. If a zero vector and an active vector are combined, the duty ratio is denoted as $d_{\rm opt}$. If two active vectors are combined, the duty ratio is denoted as $d_{\rm apt}$. A zero vector and an active vector with the optimal duty ratio $d_{\rm opt}$ and two active vectors with the optimal duty ratio $d_{\rm apt}$ have been obtained. By comparing the two voltage vector combinations, one closed to the voltage vector reference will be selected as the optimal output voltage vector combination.

As shown in the Fig. 5, the reference voltage vector is located in the second sector. In the FCS-MPC, the basic voltage vector V_2 or V_3 with a fixed direction and constant amplitude will be exerted. In the proposed method, the synthesized voltage vector goes along the direction of V_2 and V_3 when the combination of active voltage vector and zero voltage vector is applied. Thus, the degree of freedom of amplitude voltage vector is increased. When both the two active voltage vectors V_2 and V_3 are applied, the direction of the synthesized voltage vector can be changed between V_2 and V_3. Thus, the degree of phase freedom of voltage vector is increased. In can be conclude that the proposed method can simultaneously increase the degrees of the amplitude and phase freedom of the output voltage, reducing the control error of the output current.

IV. Experiment Results

The experiment is made to verify that the proposed method can obtain good performance in the output current and the inductor current to reduce the side effect of the fluctuations in photovoltaic power generation on the output power. The experimental platform of three-phase BES-qZSI has been set up, as shown in Fig. 6. The microcontroller of the experimental test is the TI digital signal processor TMS320F28335. The sampling frequency is 60 μs. The power point voltage is 100 V. The inductance and capacitance of the quasi Z-source network are 1mH and 1000 μF, respectively. The load inductance and resistance are 5 mH and 10 Ω, respectively. Fig. 7 presents the overall scheme of experimental research.

A. Steady-State Experiment

In order to compare the performance of the inductor current and the output current of the proposed method and the

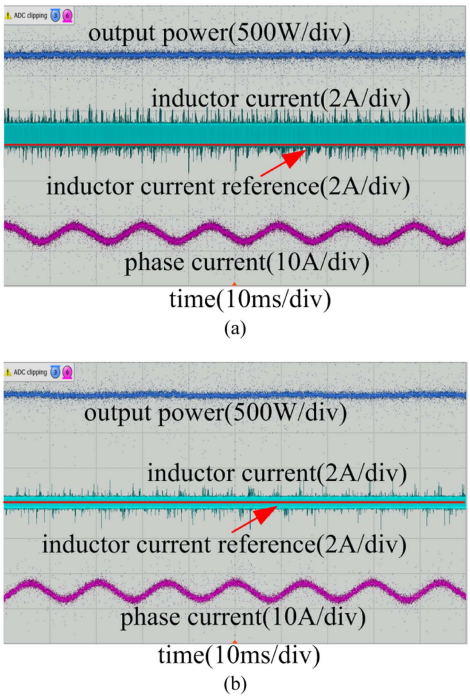

Fig. 8. Steady-state experiment results of (a) FCS-MPC and (b) proposed method.

FCS-MPC, the steady-state experiment is made by setting the reference command of the inductor current to 2 A and that of the output current to 3.75 A. The experiment results are shown in Fig. 8. It can be seen that the output powers of the two methods are all controlled a constant. The peak output currents of the two methods are about 3.8A, which is consistent with the reference command. However, the THD of the output current in the proposed method is 4%, lower that in the FCS-MPC (6%). Moreover, the ripple of the output current of the proposed method is greatly reduced, as the average value is effectively controlled. Thus, the inductor current of the proposed method has a better performance than that of the FCS-MPC. From the steady-state experiment, it is concluded that the BES-qZSI can obtain good performance by using both the proposed method and the FCS-MPC. By contrast, the proposed method has more advantage in current control than the FCS-MPC.

From the steady-state experimental results, it can be seen that the control accuracy of the proposed method is higher than that of the FCS-MPC. To facilitate observe the effect of sampling frequency on the control accuracy, the steady experiment results of the proposed method and the FCS-MPC under different sampling frequency are given in Tables I and II, respecively. It can be concluded that the proposed method has lower THD in output current, lower inductor current ripple, and accuracy control in average inductor current than the FCS-MPC.

B. Transient Experiment of Step Change in the Photovoltaic Power

To verify the performance of the suppress fluctuations in photovoltaic power, the transient performance of the proposed

TABLE I
CONTROL ACCURACY OF THE PROPOSED METHOD

Sampling frequency	THD	Inductor current ripple	Average inductor current
40 μs	4%	0.52 A	2.1 A
60 μs	4.9%	0.76 A	2.2 A
80 μs	6.1%	1.12 A	2.2 A

TABLE II
CONTROL ACCURACY OF FCS-MPC

Sampling frequency	THD	Inductor current ripple	Average inductor current
40 μs	6%	1.08 A	2.42 A
60 μs	7.2%	1.53 A	2.63 A
80 μs	8.8%	2.08 A	2.98 A

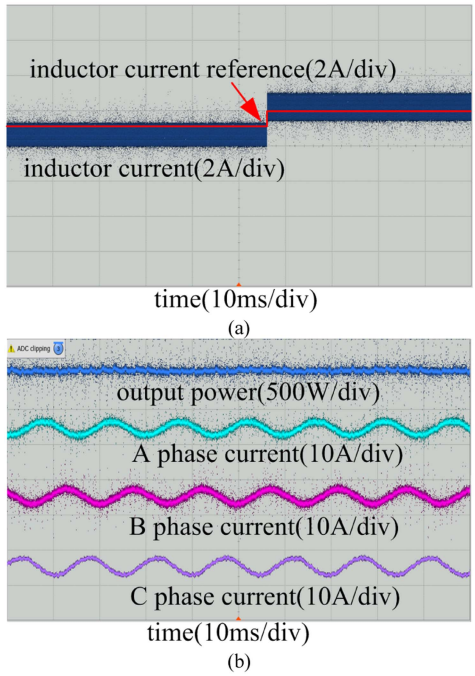

Fig. 9. Experiment results of step change in the photovoltaic power using FCS-MPC. (a) Inductor current waveform. (b) Output current and power waveforms.

method and the FCS-MPC is checked under a step change in the photovoltaic power reference, as shown in Figs. 9 and 10. The output power of the BES-qZSI is unchanged, while the photovoltaic power reference is changed from 300W to 400W in the experiment. Thus, reference command of the inductor current will increase from 3A to 4A.

It can be seen from Figs. 9 and 10 that the inductor currents of the two methods can track their references very well, obtaining fast transient behavior. Since the proposed method has a precise control for the average value of the inductor current, the average inductor current is equal to the reference command. By contrast, the average inductor current of the FCS-MPC seriously deviates from the reference command, resulting in a decline in power

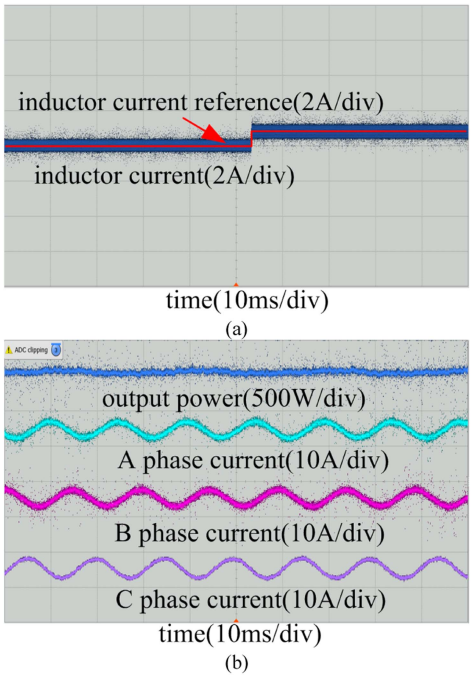

Fig. 10. Experiment results of step change in the photovoltaic power using proposed method. (a) Inductor current waveform. (b) Output current and power waveforms.

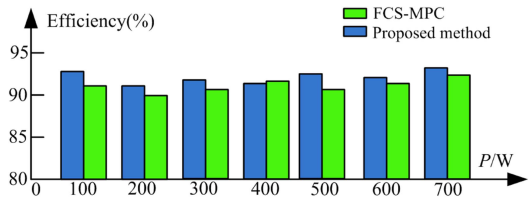

Fig. 11. Efficiencies of the BES-qZSI using the proposed method and the conventional FCS-MPC.

control. On the other hand, the inductor current ripple of the proposed method is lower than that of the FCS-MPC under any photovoltaic power. The three-phase output current as well as the output power of the BES-qZSI is not affected by the change of photovoltaic power, which indicates that the control effectiveness in power balance.

From the experimental test results, the efficiencies of the BES-qZSI using the proposed method and the conventional FCS-MPC are given in Fig. 11. It can be concluded that: the efficiencies of the BES-qZSI at different powers are all above 89% and the efficiency of the proposed method is 1%–2% higher than that of the FCS-MPC.

C. Transient Experiment of Step Change in the Output Power of BES-qZSI

The experiment of a step change in the output power of BES-qZSI is made to check the dynamic performance of power control. The power is changed from 210 to 370 W, and thus the reference command of the output current increases from 3.75 to 5 A.

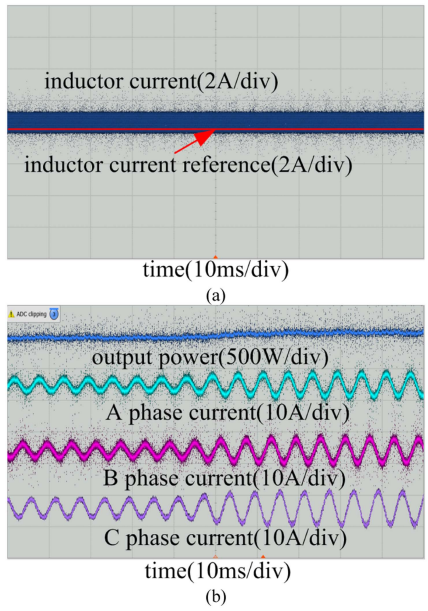

Fig. 12. Experiment results of step change in the output power using FCS-MPC. (a) Inductor current waveform. (b) Output current and power waveforms.

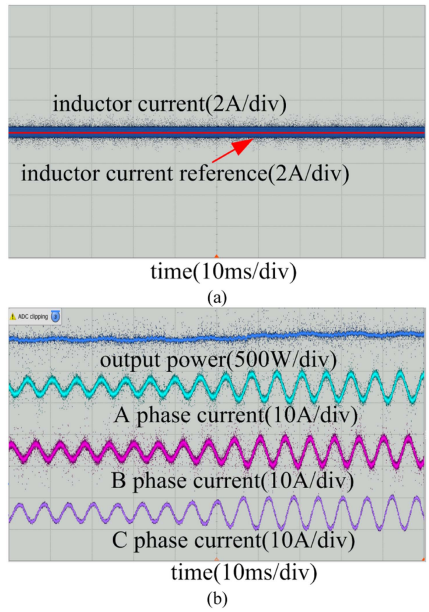

Fig. 13. Experiment results of step change in the output power using proposed method. (a) Inductor current waveform. (b) Output current and power waveforms.

From the experiment results showed in Figs. 12 and 13, it can be seen that the output currents of the two methods can quickly follow their reference command, causing an output power increase. However, the THD of output current of the proposed method is lower than that of the FCS-MPC. In addition, it can be noted that a precise inductor current is obtained using the proposed method. While the average inductor current is all lower than its reference command when using the FCS-MPC.

V. Conclusion

In order to suppress the fluctuation in photovoltaic power and improve control accuracy of the output power of the BES-qZSI, this article proposed a high-precision model predictive power control method for the BES-qZSI. The modified deadbeat control for the inductor current is achieved through alternatively applying non-shoot-through state and shoot-through state. Therefore, the average inductor current is equal to its reference command with lower ripple. The extended dual-vector model predictive control is used to supplement an active voltage vector combination into the candidate group. Hence, the output current obtains a low THD by increasing the degrees of freedom of the amplitude and phase in the output voltage. The experiment results verified that high control precise of the inductor current and the output current is obtained using the proposed method. In addition, the photovoltaic power generation system has strong robustness against the fluctuations in photovoltaic power generation.

References

[1] D. Sun, B. Ge, W. Liang, H. Abu-Rub, and F. Z. Peng, "An energy stored quasi-Z-source cascade multilevel inverter-based photovoltaic power generation system," *IEEE Trans. Power Electron.*, vol. 62, no. 9, pp. 5458–5467, Sep. 2015.

[2] O. Ellabban and H. Abu-Rub, "Z-source inverter: Topology improvements review," *IEEE Ind. Electron. Mag.*, vol. 10, no. 1, pp. 6–24, Mar. 2016.

[3] Y. He, Y. Xu, and J. Chen, "Improved space vector modulation of quasi Z-source inverter to suppress dc-link voltage sag," *IEEE Access*, vol. 7, pp. 66689–66702, May 2019.

[4] B. Ge, Y. Liu, H. Abu-Rub, and F. Z. Peng, "State-of-charge balancing control for a battery-energy-stored quasi-Z-source cascaded-multilevel-inverter-based photovoltaic power system," *IEEE Trans. Ind. Electron.*, vol. 65, no. 3, pp. 2268–2279, Mar. 2018.

[5] B. Ge et al., "An energy-stored quasi-Z-source inverter for application to photovoltaic power system," *IEEE Trans. Ind. Electron.*, vol. 60, no. 10, pp. 4468–4481, Oct. 2013.

[6] W. Liang, Y. Liu, and Y. Shen, "Active power control integrated with reactive power compensation of battery energy stored quasi-Z source inverter PV power system operating in VSG mode," *IEEE J. Emerg. Sel. Topics Power Electron.*, vol. 11, no. 1, pp. 339–350, Feb. 2023.

[7] S. Hu, Z. Liang, and X. He, "Research on the dynamic characteristics and regulation method of the energy stored quasi-Z-source inverter system," *IEEE Trans. Ind. Electron.*, vol. 67, no. 6, pp. 4590–4599, Jun. 2020.

[8] W. Liang, Y. Liu, R. Fang, and J. Peng, "Investigation on amplitude-domain modulation for three-phase energy-stored quasi-Z source inverter," *IEEE J. Emerg. Sel. Topics Power Electron.*, vol. 10, no. 3, pp. 2764–2775, Jun. 2022.

[9] Y. Liu, B. Ge, H. Abu-Rub, and F. Z. Peng, "Control system design of battery-assisted quasi-Z-source inverter for grid-tie photovoltaic power generation," *IEEE Trans. Sustain. Energy*, vol. 4, no. 4, pp. 994–1001, Oct. 2013.

[10] W. Liang, Y. Liu, B. Ge, H. Abu-Rub, R. S. Balog, and Y. Xue, "Double-line-frequency ripple model, analysis, and impedance design for energy-stored single-phase quasi-Z-source photovoltaic system," *IEEE Trans. Ind. Electron.*, vol. 65, no. 4, pp. 3198–3209, Apr. 2018.

[11] M. Mosa, R. S. Balog, and H. Abu-Rub, "High performance predictive control of quasi impedance source inverter," *IEEE Trans. Power Electron.*, vol. 32, no. 4, pp. 3251–3261, Apr. 2017.

[12] P. Karamanakos, A. Ayad, and R. Kennel, "A variable switching point predictive current control strategy for quasi-Z-source inverters," *IEEE Trans. Ind. Appl.*, vol. 54, no. 2, pp. 1469–1479, Mar./Apr. 2018.

[13] A. Ayad, P. Karamanakos, and R. Kennel, "Direct model predictive current control strategy of quasi-Z-source inverters," *IEEE Trans. Power Electron.*, vol. 32, no. 7, pp. 5786–5801, Jul. 2017.

[14] S. Sajadian and R. Ahmadi, "Model predictive-based maximum power point tracking for grid-tied photovoltaic applications using a Z-source inverter," *IEEE Trans. Power Electron.*, vol. 31, no. 11, pp. 7611–7620, Nov. 2016.

[15] S. Sajadian and R. Ahmadi, "Model predictive-based maximum power point tracking for grid-tied photovoltaic applications using a Z-source inverter," *IEEE Trans. Power Electron.*, vol. 31, no. 11, pp. 7611–7620, Nov. 2016.

[16] Y. Liu, X. Liu, X. Li, H. Yuan, and Y. Xue, "Model predictive control-based dual-mode operation of an energy-stored quasi-Z-source photovoltaic power system," *IEEE Trans. Ind. Electron.*, vol. 70, no. 9, pp. 9169–9180, Sep. 2023.

[17] A. Bakeer, M. A. Ismeil, and M. Orabi, "A powerful finite control set-model predictive control algorithm for quasi Z-source inverter," *IEEE Trans. Ind. Inform.*, vol. 12, no. 4, pp. 1371–1379, Aug. 2016.

[18] Y. Guo, H. Sun, Y. Zhang, Y. Liu, X. Li, and Y. Xue, "Duty-cycle predictive control of quasi-Z-source modular cascaded converter based photovoltaic power system," *IEEE Access*, vol. 8, pp. 172734–172746, Sep. 2020.

[19] Y. Xu, Y. He, and S. Li, "Logical operation based model predictive control for quasi Z-source inverter without weighting factor," *IEEE J. Emerg. Sel. Topics Power Electron..*, vol. 9, no. 1, pp. 1039–1051, Feb. 2021.

[20] Y. Xu, Y. He, H. Li, and H. Xiao, "Model predictive control using joint voltage vector for quasi-Z-source inverter with ability of suppressing current ripple," *IEEE J. Emerg. Sel. Topics Power Electron.*, vol. 10, no. 1, pp. 1108–1124, Feb. 2022.

[21] P. Šimek, M. Bejvl, and V. Valouch, "Power control for grid-connected converter based on generalized predictive current control," *IEEE J. Emerg. Sel. Topics Power Electron.*, vol. 10, no. 6, pp. 7072–7083, Dec. 2022.

[22] S. Jain, M. B. Shadmand, and R. S. Balog, "Decoupled active and reactive power predictive control for PV applications using a grid-tied quasi-Z-source inverter," *IEEE J. Emerg. Sel. Topics Power Electron.*, vol. 6, no. 4, pp. 1769–1782, Dec. 2018.

Yi Liu (Member, IEEE) was born in Jiangsu, China, in 1987. He received the Ph.D. degree in electrical engineering from the China University of Mining and Technology, Xuzhou, China, in 2017.

Since 2021, he has been an Associate Professor with the Institute of building intelligence, Jiangsu Vocational Institute of Architectural Technology. His research interests include power electronics, modern control theory, battery management system, and motor drives.

Jia Jia Li (Member) was born in Pingdingshan, China, in 1990. She received the master degree in electrical engineering from the China University of Mining and Technology, Xuzhou, China, in 2015.

Since 2020, she has been a Lecturer with the College of Electrical and Control Engineering, Henan University of Urban Construction. Her research interests include power electronics, renewable energy generation, and microgrid operation optimization.